Nanoparticles

DOI: 10.1002/ange.201108421

Probing Bioinspired Transport of Nanoparticles into Polymersomes**

Karmena Jaskiewicz, Antje Larsen, Ingo Lieberwirth, Kaloian Koynov, Wolfgang Meier, George Fytas, Anja Kroeger, and Katharina Landfester*

In biology the control of transmembrane transport is fundamental to functionality. The complexity of biological membranes and the diverse coupling of interactions, however, make direct investigations very difficult. Therefore the construction of synthetic artificial model membranes to study systematically their physical and chemical characteristics, and to find out how membrane functions can be modified and tuned, is of fundamental interest. Here we present a novel minimal model system, which allows the uncoupling of all interactions and processes. The model system is based on a vesicle-forming copolymer, and we report on the experimental observation of nanoparticles transport into polymersomes. A combination of photon and fluorescence correlation spectroscopies is used to study the internalization in detail. These techniques provide information about the kinetics and dynamics of this process in real time. The resulting picture is supported by cryo-TEM imaging. The new possibility of studying nanoparticle internalization processes on the basis of an artificial model system presented here opens a new pathway for the fundamental understanding, and hence control, of nanoparticle uptake processes in living cells.[1]

Transport of molecules and colloidal particles from the extracellular environment to the cell interior is mediated by different endocytotic machineries[2] and is of fundamental importance in drug delivery, nanotoxicology, and disease diagnosis.[3] Whereas in biology the term endocytosis refers to mechanisms of incorporation of molecules and particles by an invagination process assisted by biofunctional molecules and/or supplementary energy, recent studies have revealed the existence of non-endocytotic pathways for nanoscaled objects.[4] In spite of the large effort to distinguish all the factors playing a role during particle incorporation,[5] the successful description of the coordinated process is still elusive.[1,6] The key-stage of endocytosis is the invagination of the cell membrane, followed by wrapping and pinching off the particle into the interior of the cell. During this process, cells generate significant mechanical force, leading to membrane deformation.

The mechanisms behind endocytotic processes are an object of intensive theoretical studies,[7] while experimental work is missing because of the complexity of the cellular system and paucity of powerful techniques. One simple theoretical model was based on the interactions of unilamelar vesicles with colloidal particles.[8] This almost over-simplified model was able to mimic a particle internalization process driven by adhesion and mechanical properties of the bilayer, that is, fluidity and elastic moduli. The size ratio of the vesicle and internalized nanoparticle appears crucial for successful incorporation, as indicated by experiments performed on both living cells and liposomes.[9] The uptake of nanoparticles was reported to be strictly size- and shape-dependent,[1b,10] and moreover, the curvature of the bilayer strongly influences the internalization process.

Here we go one step further, demonstrating particle incorporation by artificial membranes, thus providing novel characterization possibilities of the system. We demonstrate that many detailed studies can be performed in much less complex systems than the cell. Detailed investigations of the size, shape, and surface dependence of the particle uptake can be carried out using this artificial platform and then applied in living systems. Using polymeric vesicles (polymersomes) as a cell model, we demonstrate the incorporation of polystyrene (PS) and silica (SiO_2) nanoparticles in a system free of any biofunctional molecule and/or supplementary energy.

Polymeric vesicles composed of poly(dimethylsiloxane)-*block*-poly(2-methyloxazoline) (PDMS-*b*-PMOXA)[11] were chosen as a model system of an unspecified cell membrane (Figure 1). These polymersomes are an ideal model system, as the physical properties of their building blocks (polymer chains) are similar to phospholipids. Based on the values of the Young modulus (around 17 MPa) and the bending energy (around 7×10^{-18} J), they provide the necessary fluidity of a membrane and concurrently ensure excellent mechanical stability. The latter is due to the slow exchange of polymer chains between aggregates compared to the experimental time scale (kinetically trapped or "frozen" structures). In addition, polymersomes can be easily modified in both biological and chemical respects for further investigations.

[*] K. Jaskiewicz, Dr. I. Lieberwirth, Dr. K. Koynov, Dr. A. Kroeger, Prof. K. Landfester
Max Planck Institute for Polymer Research
Ackermannweg 10, 55128 Mainz (Germany)
E-mail: kroeger@mpip-mainz.mpg.de
A. Larsen, Prof. G. Fytas
Department of Materials Science and Technology
University of Crete and F.O.R.T.H.
P.O. Box 1527, 71110 Heraklion (Greece)
Prof. W. Meier
Department of Chemistry, University of Basel
Klingelbergstrasse 80, 4056 Basel (Switzerland)

[**] This work was supported by the Max Planck Graduate Center (MPGC) through the Max Planck Society and the Johannes Gutenberg University Mainz. The authors gratefully thank Dr. Stefan Egli (University of Basel) for the synthesis of PDMS-*b*-PMOXA copolymer, Dr. Umaporn Paiphansiri for the PS nanoparticles synthesis, and Christine Rosenauer (MPI-P Mainz) for experimental support. Sulivan Vianna is kindly acknowledged for some of the artwork.

Supporting information for this article is available on the WWW under http://dx.doi.org/10.1002/anie.201108421.

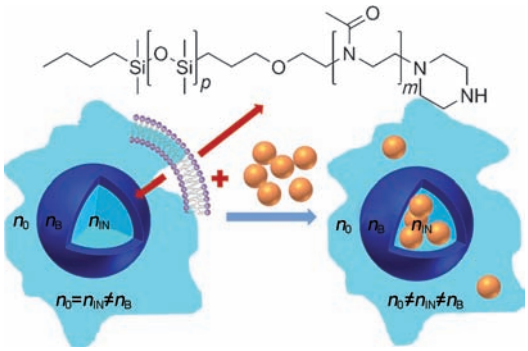

Figure 1. The chemical primary structure of poly(dimethylsiloxane)-*block*-poly(2-methyloxazoline) (PDMS-*b*-PMOXA) forming the secondary structure, polymersomes (large blue spheres), in aqueous solution. Polymersomes in the absence (left) and the presence of nanoparticles symbolized by orange spheres (right). Refractive indices of the solvent (water, n_0), diblock copolymer bilayer (n_B), and polymersome interior (n_{IN}). p and m refer to the degree of polymerization ($p=68$, $m=11$).

By using an extrusion technique[12] polymersomes with a hydrodynamic radius, R_h, of around 100 nm were deliberately prepared to optimally use the present techniques. This vesicle size leads to a low polydispersity, resulting in a better control of the system. These polymersomes combined with PS nanoparticles of $R_h=(16\pm1)$ nm or SiO_2 nanoparticles with $R_h=(14\pm1)$ nm constituted the minimal model system for the investigation of adsorption and transmembrane transport. The experiments were performed in aqueous solution without any additives, allowing the vesicle–particle interactions to be exclusively studied.

To visualize adsorption and internalization of nanoparticles by polymeric vesicles, cryogenic transmission electron microscopy (cryo-TEM) images of the polymersome solutions containing either PS or SiO_2 nanoparticles were acquired (Figure 2). As shown in Figure 2, PDMS-*b*-PMOXA polymersomes incorporate both types of nanoparticles through an invagination process by membrane

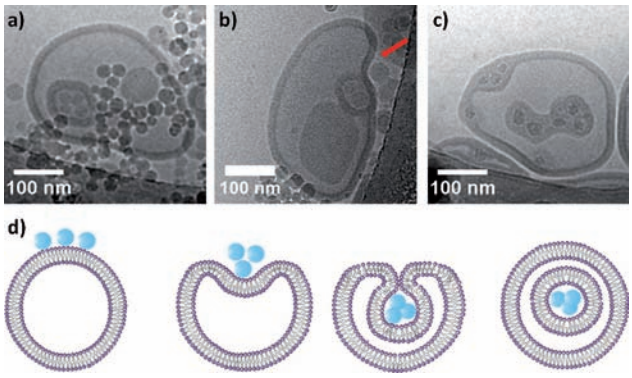

Figure 2. Cryo-TEM micrographs of nanoparticles inside PDMS-*b*-PMOXA polymersomes. a–c) Internalization of PS nanoparticles $R_h=16$ nm (a, b) and SiO_2 nanoparticles $R_h=14$ nm (c). d) Schematic illustration of nanoparticle internalization into polymersome. The nanoparticles are first absorbed, then wrapped by the polymeric membrane (red arrow), and finally completely incorporated.

deformation and subsequent fission of the bilayer membrane. This process can be described in four steps: 1) nanoparticle adsorption at the vesicle surface (Figure 2a), 2) engulfing of single nanoparticles or groups of particles (Figure 2b and c) by wrapping and formation of necks, 3) entire coverage of the nanoparticles by the bilayer membrane (Figure 2b), and 4) complete internalization (Figure 2a and c) driven by the antagonistic effects of the bending and adhesion energies; an additional contribution might arise from the entropy gain through release of water from the nanoparticle surface.[13] Figure 2d is a schematic description of this process.

Cryo-TEM imaging provides a direct static picture of the system. However, as the sample is investigated in a frozen state, information on the dynamics of the process is lost. Furthermore, in the TEM studies shown above, only a relatively small number of individual structures can be evaluated statistically. To overcome these limitations, we favored photon correlation spectroscopy (PCS), a noninvasive light scattering technique with broad spatiotemporal range.[14] In contrast to TEM, PCS measurements integrate over a large number of scattering centers. The application of PCS to the present system is optimal due to the mesoscopic lengths of the involved species and the large optical contrast between them and the solvent. Polymeric vesicles suspended in water have an inner and outer refractive index ($n_{IN}=n_0$) equal to water ($n=1.333$). As illustrated in Figure 1 however, the invagination of particles ($n_{PS}=1.59$ and $n_{SiO_2}=1.45$) will significantly change the refractive index of the polymersome interior n_{IN}, and hence the total light scattering intensity. Further, the combination of large optical contrast and a core–shell architecture of the polymersomes will render both the form factor $P(q)$ and the translational diffusion $D(q)$ sensitive indices of the uptake process. The variation of the excess absolute time-average scattered intensity, known as the Rayleigh ratio $R_{vv}(q)$ (around $P(q)$) and $D(q)$ with the probing wave vector q, fully characterizes the polymersome dilute solution with a z-average radius $R_h=(112\pm3)$ nm, size polydisdipersity $PD=1.1$, and a bilayer thickness d of 14 nm (Figure 3).

For the particle internalization experiments, a dilute aqueous polymersome solution (polymer concentration $c_P=4.5\times10^{-2}\,g\,L^{-1}$) was mixed with a nanoparticle dispersion (nanoparticle concentration $c_{NP}=0.1\,g\,L^{-1}$) at a number ratio 1:50 and then immediately probed by PCS (Figure 3). The initially low light scattering intensity (at $q=0.024\,nm^{-1}$) jumped to a much higher level, displaying strong fluctuations with elapsed time, and finally reached a plateau, as seen in Figure 3a for the PS ($R_h=16$ nm) and Figure 3d for SiO_2 ($R_h=14$ nm) nanoparticles. For both mixtures, the final scattering intensity is much higher than the sum of the scattering intensity contributions from the individual components and was significantly higher in the case of the PS/polymersome system (around 10 times higher) compared to SiO_2/polymersome system (around 2 times higher) as seen in Figure 3 (Figure S2 in the Supporting Information for details). The equilibration time was much shorter in the case of the SiO_2 nanoparticles (around 8 min), suggesting much faster internalization kinetics than in the case of the PS nanoparticles (around 15 min) with a similar size (Figure 3a and

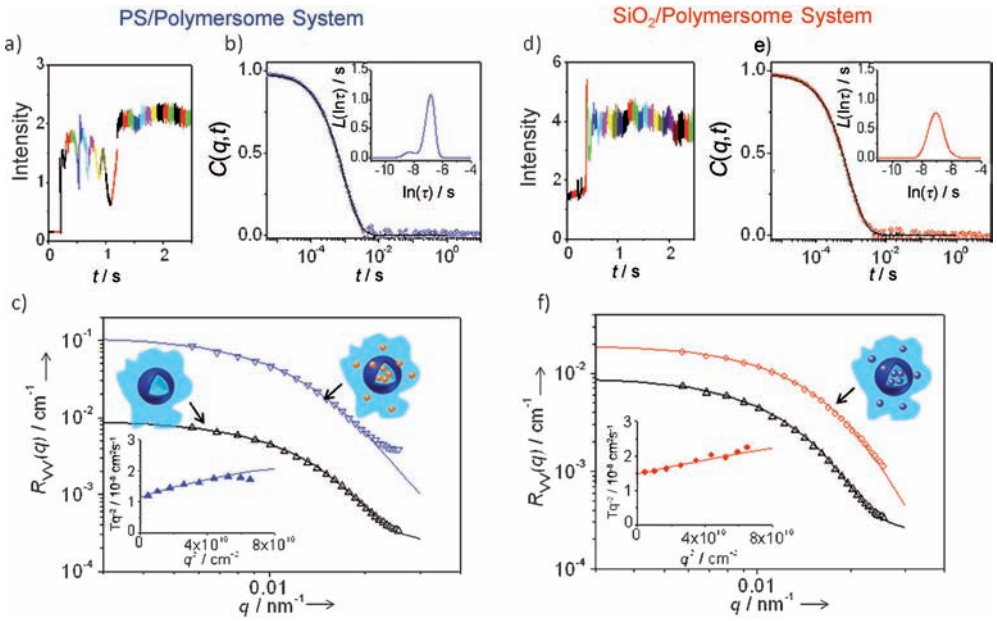

Figure 3. Nanoparticle incorporation into PDMS-*b*-PMOXA polymersomes measured by PCS. a) Total light scattering intensity at a scattering wave vector $q = 0.024$ nm^{-1} as a function of time after the addition of a PS nanoparticle suspension to the aqueous polymersome solution. Within the colored sections the dynamic state of the mixture was probed. b) Normalized field autocorrelation functions $C(q,t)$ of the PS/polymersome system at a scattering wave vector $q = 0.024$ nm^{-1} (diffusion length around 260 nm) along with the corresponding distribution of relaxation times $L(\ln\tau)$ recorded after 2 h. c) Absolute light scattering intensity (black triangles: empty polymersomes, blue inverse triangles: PS/polymersome system) and the $D(q)$ (filled symbols) fitted by the corresponding form factor function (solid lines). d–f) The equivalent plots for the SiO_2/polymersome system (empty and filled red circles, black triangles: empty polymersomes). The state of the examined solution is schematically indicated in the insets of (c) and (f).

d). We assume the same uptake mechanism (Figure 2) for both particles possessing, however, a distinct surface chemistry. Therefore, the disparity in the internalization kinetics can be related to the different strengths of the particle–membrane adhesive interactions.

The experimental $R_{vv}(q)$ and $D(q)$ values were obtained from the concentration relaxation functions $C(q,t)$ which were represented by a unimodal distribution function $L(\ln\tau)$ as seen in Figure 3 b and e. Freely diffusing nanoparticles were observed (weak peak in $L(\ln\tau)$ of Figure 3 b) only in the PS/polymersome system because of the much larger optical contrast of PS compared to the SiO_2 nanoparticles. The single diffusional decay rate, $\Gamma(q) = D(q)q^2$, corresponding to the main peak of $L(\ln\tau)$, was used to compute the effective $D(q)$ shown in the insets of Figure 3 c and f for the two different systems. Assuming that polymersomes are filled with nanoparticles (schematically shown in Figure 1), both experimental quantities, $R_{vv}(q)$ and $D(q)$, were well represented by an appropriate form factor termed filled vesicle model (see the Methods Section in the Supporting Information for details). An alternative model of a decorated vesicle (the particles are attached to the outer surface of the polymersomes) fails to describe the experimental intensity pattern (see the Supporting Information for details). Therefore, it appears that after an equilibration time most of the polymersomes internalized nanoparticles. The moderate representation of the experimental $R_{VV}(q)$ for the PS/polymersome system at the highest q values (Figure 3 c) by the filled vesicle model is ascribed to the inhomogenity of the moieties which comprises different filled vesicles (number of internalized particles) and freely diffusing PS nanoparticles; in the case of SiO_2 nanoparticles (with lower optical contrast) this contribution of system polydispersity and free nanoparticles is suppressed (Figure 3 f).

The simultaneous description of both $R_{vv}(q)$ and $D(q)$ depends sensitively on the refractive index n_{IN} in the interior of the polymersomes, in addition to their average radius and size polydispersity. Since the latter two do not change significantly compared to the empty polymersomes, it is mainly the increase of n_{IN} above the pure water value that boosts the intensity $R_{vv}(0)$ as shown in Figure 3. From the data representation by the filled vesicle model, the values $n_{IN} = 1.38 \pm 0.01$, for polymersomes filled with SiO_2 ($R_h = 14$ nm) and $n_{IN} = 1.41 \pm 0.01$, for polymersomes filled with PS ($R_h = 16$ nm) nanoparticles, correspond to about 40 and 30 % particle loading of the vesicles interior, respectively. The average size of loaded polymersomes was found to be about 10 % smaller than the unloaded species corresponding to around 20 % volume shrinkage. This is in accord with the average number of internalized particles and the associate membrane consumption (Figure 2).

A comparison with the extent of the internalization observed by cryo-TEM (Figure 2) is not straightforward because of the strong concentration dependence of the internalization process. The very low concentrations in PCS experiments are not sufficient for cryo-TEM imaging which required a much higher nanoparticle/polymersome concentration. Instead, we employed fluorescence correlation spectroscopy (FCS) under PCS experimental conditions and used labeled nanoparticles.

In a FCS experiment, the fluorescent intensity fluctuations caused by the diffusion of fluorescent species through a very small observation volume (the focus of a confocal microscope) are monitored. Correlation analysis of these fluctuations yields information on the hydrodynamic radius of the species, their concentration, and fluorescent brightness (see the Methods Section in the Supporting Information for details). Figure 4 presents typical fluorescence intensity autocorrelation functions $G(t)$ recorded at different times after the injection of the fluorescent PS nanoparticle suspen-

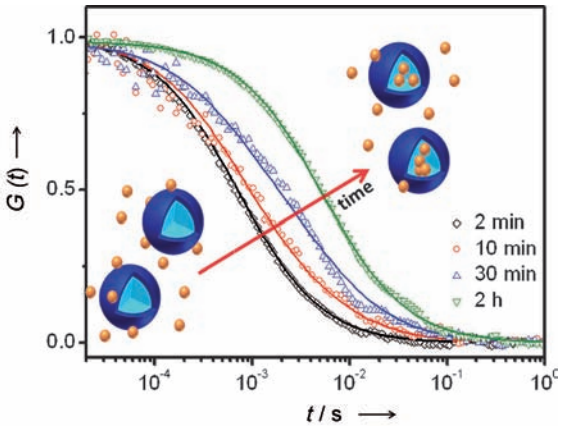

Figure 4. Kinetics of the loading of PS nanoparticles into PDMS-*b*-PMOXA polymersomes probed by FCS. The experimental autocorrelation functions (symbols) recorded by fluorescence correlation spectroscopy (FCS) at different times (2 min–2 h) after mixing the PS ($R_h = 16$ nm) nanoparticles and polymersome solutions are given (solid lines) by Equation (5) in the Supporting Information, using either a one component diffusing model (black and green curves) or a two component model (red and blue).

sion into the polymersome solution. Clearly, the autocorrelation curves progressively shift to longer diffusion times, indicating larger species with increased exposure time. FCS monitors only the fluorescently labeled PS beads, either freely diffusing or incorporated in the larger polymer vesicles. The early and late stage curves (Figure 4, black and green symbols) are well represented by a single diffusing moiety (see the Methods Section in the Supporting Information) with $R_h = 16$ and 95 nm, respectively. These radii correspond to the free PS nanoparticles in the initial stage (2 min) and to the polymer vesicles loaded with PS nanoparticles at the late stage (around 2 h) of the loading process. From the average fluorescent brightness of the PS beads and the loaded polymersomes we estimated a loading of about 16 incorporated particles per polymeric vesicle, which is in agreement with the PCS value. The experimental $G(t)$ recorded after 10 and 30 min (Figure 4, red and blue symbols) can be represented by two diffusive decays (see the Methods Section in the Supporting Information), corresponding to freely diffusing PS beads with $R_h = 16$ nm and loaded polymer vesicles with $R_h = 95$ nm. The latter value is similar to the radius obtained using PCS. From the relative contributions of the two decays to $G(t)$, the number ratio of these two species is estimated as 4 and 0.8 after 10 and 30 min of loading, respectively. At the latest state the contribution from individual particles is hardly resolved mainly because of the much higher fluorescent brightness of the loaded vesicles relative to the free nanoparticles. Thus FCS is a suitable complementary technique to follow the kinetics of particle loading into polymersomes smaller than the probing area, and possibly to follow particle motion inside the polymeric vesicles (Figure 1) for larger polymersome sizes.

Transmembrane transport of nanoparticles can be imitated by an artificial polymeric membrane system with suitably designed physical parameters. The process itself can be driven by physical parameters of the system even when cell membrane proteins and other bioactive components as well as supplementary energy are missing. Here, because of the absence of any external stimuli, curvature-mediated attractive interactions (strong adhesive interactions) between nanoparticles and polymersomes are assumed to be the driving force for this process. A balance between the fluidity of the membrane and a short-ranged adhesive potential, given by the critical ratio of the geometric radii of the nanoparticles and polymersomes, is of importance. The fact that transmembrane transport of nanoparticles can be performed by artificial model system without any additional stimuli has a fundamental impact on the understanding, not only of the nanoparticle invagination process but also of the interaction of nanoparticles with biological as well as polymeric membranes. The designed minimal model system will be further modified and specialized to finally provide a generic platform for fundamental understanding, and an efficient tool for the preparation of smart nanoscaled systems for biomedical applications and nanotoxicology research.

Received: November 29, 2011
Revised: February 28, 2012
Published online: March 30, 2012

Keywords: endocytosis · nanoparticles · polymers · supramolecular chemistry

[1] a) E. C. Cho, Q. Zhang, Y. Xia, *Nat. Nanotechnol.* **2011**, *6*, 385–391; b) W. Jiang, B. Y. S. Kim, J. T. Rutka, W. C. W. Chan, *Nat. Nanotechnol.* **2008**, *3*, 145–150.

[2] a) S. D. Conner, S. L. Schmid, *Nature* **2003**, *422*, 37–44; b) M. Lakadamyali, M. J. Rust, X. Zhuang, *Microbes Infect.* **2004**, *6*, 929–936.

[3] a) K. Roy, H. Q. Mao, S. K. Huang, K. W. Leong, *Nat. Med.* **1999**, *5*, 387; b) T. J. Yoon, J. S. Kim, B. G. Kim, K. N. Yu, M. H. Cho, J. K. Lee, *Angew. Chem.* **2005**, *117*, 1092–1095; *Angew. Chem. Int. Ed.* **2005**, *44*, 1068–1071.

[4] a) C. J. Merrifield, M. E. Feldman, L. Wan, W. Almers, *Nat. Nanotechnol.* **2002**, *4*, 691–698; b) G. A. Jonsdottir, R. Li, *Curr. Biol.* **2004**, *14*, 1604–1609; c) B. M. Rothen-Rutishauser, S. Schürch, B. Haenni, N. Kapp, P. Gehr, *Environ. Sci. Technol.* **2006**, *40*, 4353–4359; d) C. Liu, X. Zhen, X. Wang, W. Wu, X. Jiang, *Soft Matter* **2011**, *7*, 11526–11534.

[5] a) S. M. Sweitzer, J. E. Hinshaw, *Cell* **1998**, *93*, 1021–1029; b) C. J. Merrifield, D. Perrais, D. Zenisek, *Cell* **2005**, *121*, 593–606.

[6] H. D. Summers, P. Rees, M. D. Holton, M. R. Brown, S. C. Chappell, P. J. Smith, R. J. Errington, *Nat. Nanotechnol.* **2011**, *6*, 170–174.

[7] a) G. Illya, R. Lipowsky, J. Shillcock, *J. Chem. Phys.* **2005**, *122*, 244901; b) M. Fošnarič, A. Iglič, D. M. Kroll, S. May, *J. Chem. Phys.* **2009**, *131*, 105103; c) C. Dietrich, M. Angelova, B. Pouligny, *J. Phys. II* **1997**, *7*, 1651–1682.

[8] a) M. Deserno, W. M. Gelbart, *J. Phys. Chem. B* **2002**, *106*, 5543–5552; b) M. Deserno, T. Bickel, *Europhys. Lett.* **2003**, *62*, 767.

[9] O. Le Bihan, P. Bonnafous, L. Marak, T. Bickel, S. Trépout, S. Mornet, F. De Haas, H. Talbot, J. C. Taveau, O. Lambert, *J. Struct. Biol.* **2009**, *168*, 419–425.

[10] a) B. D. Chithrani, A. A. Ghazani, W. C. W. Chan, *Nano Lett.* **2006**, *6*, 662–668; b) B. D. Chithrani, W. C. W. Chan, *Nano Lett.* **2007**, *7*, 1542–1550; c) B. J. Reynwar, G. Illya, V. A. Harmandaris, M. M. Muller, K. Kremer, M. Deserno, *Nature* **2007**, *447*, 461.

[11] S. Egli, M. G. Nussbaumer, V. Balasubramanian, M. Chami, N. Bruns, C. Palivan, W. Meier, *J. Am. Chem. Soc.* **2011**, *133*, 4476 – 4483.
[12] F. Olson, C. Hunt, F. Szoka, W. Vail, D. Papahadjopoulos, *Biochim. Biophys. Acta Biomembr.* **1979**, *557*, 9 – 23.
[13] K. A. Smith, D. Jasnow, A. C. Balazs, *J. Chem. Phys.* **2007**, *127*, 084703.
[14] a) J. Pencer, F. R. Hallett, *Langmuir* **2003**, *19*, 7488 – 7497; b) A. Kroeger, V. Deimede, J. Belack, I. Lieberwirth, G. Fytas, G. Wegner, *Macromolecules* **2007**, *40*, 105 – 115.

